(Preprint) AAS 19-371

GRAVITATIONAL CAPTURE AT SATURN WITH LOW-THRUST ASSISTANCE

E. Fantino[*], J. Peláez[†], R. Flores[‡], and V. Raposo-Pulido[§]

Orbit insertion at Saturn requires a large manoeuver with chemical thrusters to compensate for the velocity difference between the spacecraft and the planet. The impact that this has on the propellant budget is severe. This paper discusses an alternative strategy: after a gravity assist with Jupiter, an electrical motor with an *ad hoc* thrusting law reshapes the orbit and minimizes the hyperbolic excess speed at Saturn, thus facilitating the capture. The control law algorithm, as well as the dynamical and technological aspects are presented and discussed.

INTRODUCTION

The outer planets are of particular interest in terms of what they can reveal about the origin and evolution of our solar system. They are also local analogues for many extra-solar planets that have been detected over the past twenty years. The study of these planets furthers our comprehension of our neighborhood and provides the foundations to understand distant planetary systems. The giant planet satellites have their own special place in our quest for learning about our origins and our search for life, and robotic missions are essential tools for this scientific goal. Missions to the outer planets have been prioritized by NASA and ESA, and this has resulted in important space projects for the exploration of the Jupiter's system, such as NASA's Europa Clipper and the ESA's Jupiter Icy Moons Explorer.[1,2] Note that no mission to Uranus or Neptune has ever been undertaken due to the prohibitive amount of propellant required to decelerate and get captured by the planets' gravity upon arrival from an interplanetary trajectory. In fact, insertion into orbit around any outer planet is highly demanding in terms of propellant. Cassini/Huygens travelled to Saturn following a ΔV-VVEJGA trajectory. The hyperbolic excess speed at Saturn was higher than 5 km/s. Orbit insertion (OI) was performed with a bipropellant engine which burnt more than 800 kg of fuel during 1.5 hours causing a velocity variation of 622 m/s.[3] The subsequent pericenter raising maneuver added another 300 kg to the amount of consumed propellant. Additionally, over 1000kg of propellant were required for deep space maneuvers and course corrections before OI. It is clear that the impact of these operations on the size and overall cost of the mission was severe. One alternative to reduce

[*] Assistant Professor, Aerospace Engineering Department, Khalifa University of Science and Technology, P.O. Box 127788 Abu Dhabi, United Arab Emirates. Research Fellow, Space Dynamics Group, School of Aeronautical and Space Engineering, Technical University of Madrid, Plaza Cardenal Cisneros 3, 28040 Madrid, Spain.

[†] Professor, Space Dynamics Group, School of Aeronautical and Space Engineering, Technical University of Madrid, Plaza Cardenal Cisneros 3, 28040 Madrid, Spain. Visiting Scholar, Aerospace Engineering Department, Khalifa University of Science and Technology, P.O. Box 127788 Abu Dhabi, United Arab Emirates.

[‡] Associate Professor, International Center for Numerical Methods in Engineering, Campus Norte UPC, Gran Capitán s/n, 08034 Barcelona, Spain.

[§] PhD Candidate, Space Dynamics Group, School of Aeronautical and Space Engineering, Technical University of Madrid, Plaza Cardenal Cisneros 3, 28040 Madrid, Spain.

the cost of exploring the giant planets is to use low-energy transfers between libration point orbits.[4] An application of this concept aided by low-thrust propulsion can be found in Reference 5. While extremely energy-efficient, the very long duration of the transfer renders this approach impractical for realistic missions. Another alternative is using the Lorentz-force interaction with a planetary magnetic field to produce thrust. In standard spacecraft (S/C), the interaction reduces to magnetic torques and only the effect on spacecraft attitude is relevant.[6,7] However, by using an electrodynamic tether (ET), a significant thrust force can be produced to assist in orbit insertion.[8] Whereas use of the ET is readily possible for Jupiter,[9] the case for the other three outer planets presents issues because the efficiency of spacecraft capture with an ET is inversely proportional to the square of the magnitude of the planetary magnetic field, which is remarkably weak at Saturn, Uranus and Neptune. However, in the specific case of Saturn, if the relative velocity between the S/C and Saturn at the encounter is sufficiently decreased, the capture and final OI of the probe can still be achieved using the electrodynamic drag produced by the ET (see Reference 10). The ET concept paves the way towards missions to explore Saturn and its moons with S/C masses below one tonne (the mass of Cassini/Huygens at launch was 5600 kg). This enables use of smaller launchers, significantly reducing the overall mission cost.

In the present work, we investigate a method to minimize the hyperbolic excess speed upon arrival at Saturn, thus facilitating OI by means of, e.g., an ET. For the sake of simplicity and to save propellant, the type of transfer chosen to reach Saturn is a ΔV-JGA trajectory. The S/C departs from the Earth's orbit with a tangential $\Delta\mathbf{V}$ compatible with the capabilities offered by existing rockets. An unpowered gravity assist (GA) with Jupiter redirects the S/C towards Saturn, and electric propulsion provides continuous low thrust for a certain interval of time with the objective of minimizing the arrival speed at Saturn. The propulsion performance characteristics are those of the NASA Evolutionary Xenon Thruster (NEXT).[11]

Planetary orbits are assumed circular and coplanar, and the trajectory is also 2D, although the method can be easily extended to 3D. The Earth-to-Jupiter portion of the trajectory is computed with the Sun-S/C two-body model, whereas a simple patched conics approximation is adopted to describe the GA with Jupiter. Upon exiting the sphere of influence of the planet, the S/C is subjected to the gravity pull of the Sun only, supplemented by the thrust of the propulsion system over a certain time interval, at the end of which the S/C coasts to reach the orbit of Saturn. The low-thrust portion of the trajectory is optimized with respect to arrival conditions at Saturn, and this is achieved by implementing a steering law reminiscent of the Q-guidance method for missile targeting, with the hyperbolic excess velocity taking the place of the velocity-to-be-gained vector.[12] The practical implementation of the method is, in essence, an application of the classical gradient descent optimization technique.[13]

The paper is organized as follows: we first present the design of the Earth-to-Jupiter portion of the trajectory, including the GA; then we illustrate the control law algorithm, and we apply it to the Jupiter-to-Saturn transfer. A discussion of the results and some indications of future work conclude the paper.

FROM THE EARTH TO JUPITER

Earth-to-Jupiter Sun-S/C two-body ellipses are determined with a double loop over the semimajor axis a_0 of the departure heliocentric ellipse (varied between the value corresponding to the Hohmann transfer from Earth to Jupiter and 6 ua) and the perijove radius r_π of the Jupiter-centered hyperbola (varied between $0.6 \cdot 10^6$ km and 10^7 km). Additionally, the following restrictions apply:

- characteristic departure energy $C_3 < 85$ km^2/s^2, compatible with the capability of major interplanetary carrier rockets (see also Reference 14);

- perihelion at the Earth (heliocentric distance r_E = 1 ua);

The GA is modelled with the patched conics method. When the S/C crosses the orbit of Jupiter, the planet's velocity $\mathbf{V}_J$ is subtracted from the S/C velocity $\mathbf{V}^-_{S/C}$. The resulting $\mathbf{v}^-_\infty$ vector and the choice of r_π fully determine the Jupiter-centered hyperbola, in particular the relative velocity $\mathbf{v}^+_\infty$ at sphere of influence exit and the corresponding new heliocentric velocity $\mathbf{V}^+_{S/C}$ of the S/C. We assume that both the velocity of Jupiter and the heliocentric position of the S/C remain unchanged over the GA. The post-GA heliocentric elliptical orbits are divided into two groups, i.e., those which intersect the orbit of Saturn (IN) and those which do not (NI). They are treated differently by the guidance algorithm, as discussed in the next section.

Figure 1 in the Appendix summarizes the core features of the post-GA Sun-S/C two-body ellipses obtained with the above procedure. The top plot shows the hyperbolic excess speed at Saturn's orbit for set IN as a function of launch C_3 and perijove radius (expressed in units of 10^6 km and written at the cutoff of each curve). The bottom plot gives the aphelion radius of the orbits of set NI as a function of launch C_3 and perijove radius. The red solid circles identify the trajectories which, after application of the low-thrust control law (see below), give the minimum arrival excess velocity.

CONTROL LAW FOR THE LOW-THRUST TRANSFER

Nomenclature

In a Cartesian inertial reference system, let us define the state vector $\mathbf{s}$ of a point-particle as

$$\mathbf{s}(t) = \begin{bmatrix} \mathbf{r} \\ \dot{\mathbf{r}} \end{bmatrix} = \begin{bmatrix} x \\ y \\ V_x \\ V_y \end{bmatrix}. \tag{1}$$

When appropriate, we shall use polar coordinates $\{r, \theta\}$ such that

$$\mathbf{r} = r\mathbf{u}_r \;\; ; \;\; \mathbf{u}_r = \begin{bmatrix} \cos\theta \\ \sin\theta \end{bmatrix} \;\; ; \;\; \mathbf{u}_\theta = \begin{bmatrix} -\sin\theta \\ \cos\theta \end{bmatrix}. \tag{2}$$

The particle moves under the gravitational attraction of a central body, characterized by its gravitational parameter μ. The central body is located at the origin of the reference frame. Furthermore, there is a propulsion system capable of producing a specific thrust (i.e., acceleration)

$$\mathbf{f}(t) = f_r\mathbf{u}_r + f_\theta\mathbf{u}_\theta. \tag{3}$$

Thus, the system of governing equations is

$$\frac{\mathrm{d}\mathbf{s}}{\mathrm{d}t} = \begin{bmatrix} V_x \\ V_y \\ a_x \\ a_y \end{bmatrix} \text{ where } \mathbf{a} = \left(f_r - \frac{\mu}{r^2}\right)\mathbf{u}_r + f_\theta\mathbf{u}_\theta. \tag{4}$$

At each point in time, we shall define a vector of osculating Keplerian elements

$$\mathbf{o}(\mathbf{s}) = \begin{bmatrix} a \\ e \\ \omega \\ M_0 \end{bmatrix}. \tag{5}$$

The components of the vector are the semimajor axis a, the eccentricity e, the longitude of the pericenter ω and the mean anomaly M_0 at epoch, respectively. In the following, we shall focus on a and e exclusively, but the procedure is applicable to all four elements.

Problem statement

Given a system governed by Eq. (4), an initial state vector $\mathbf{s}(0) = \mathbf{s}_0$ and an error function $\Im$ expressed in terms of the osculating orbital elements (i.e., $\Im(\mathbf{o})$); find a control law $\mathbf{f}(t)$ that minimizes the error function in the shortest time, subject to the constraint $|| \mathbf{f} || \leq f_{max}$ (i.e., the available thrust is fixed).

Optimal control law

We shall assume that the optimal guidance strategy is the one that maximizes the instantaneous rate of reduction of the error function $\Im(a, e)$. As the magnitude of the thrust f_{max} is very small compared to the gravitational pull of the Sun, the effect of the propulsion system can be linearized (i.e., the rate of change of $\Im$ is a homogenous function of the thrust components). Thus, to achieve the fastest reduction of $\Im$, the maximum thrust has to be used at all times. The only free parameter is the orientation of the thrust vector (β)

$$\mathbf{f} = f_{\max} \left(\sin\beta \, \mathbf{u}_r + \cos\beta \, \mathbf{u}_\theta \right). \tag{6}$$

The optimal control law is determined by the conditions

$$\frac{\partial}{\partial \beta} \left[\frac{\mathrm{d}\Im\left(\mathbf{o}(\mathbf{s})\right)}{\mathrm{d}t} \right] = 0 \quad \text{and} \quad \frac{\mathrm{d}\Im\left(\mathbf{o}(\mathbf{s})\right)}{\mathrm{d}t} < 0. \tag{7}$$

We compute the rate of change of the error using the chain rule:

$$\frac{\mathrm{d}\Im\left(\mathbf{o}(\mathbf{s})\right)}{\mathrm{d}t} = \nabla\Im^T \cdot \frac{\mathrm{d}\mathbf{o}}{\mathrm{d}t}. \tag{8}$$

For our particular case, where $\Im(\mathbf{o}) = \Im(a, e)$, the gradient is

$$\nabla\Im = \begin{bmatrix} \frac{\partial\Im}{\partial a} \\ \frac{\partial\Im}{\partial e} \end{bmatrix}. \tag{9}$$

The rate of change of the orbital elements can be expressed in matrix form as

$$\frac{\mathrm{d}\mathbf{o}}{\mathrm{d}t} = \begin{bmatrix} \dot{a} \\ \dot{e} \end{bmatrix} = \begin{bmatrix} \frac{\partial\dot{a}}{\partial f_r} & \frac{\partial\dot{a}}{\partial f_\theta} \\ \frac{\partial\dot{e}}{\partial f_r} & \frac{\partial\dot{e}}{\partial f_\theta} \end{bmatrix} \cdot \begin{bmatrix} f_r \\ f_\theta \end{bmatrix} = \mathbf{R} \cdot \mathbf{f}. \tag{10}$$

The components of matrix $\mathbf{R}$ are computed from Gauss' planetary equations

$$\frac{\partial \dot{a}}{\partial f_r} = c_1\, e\, \sin\nu\,, \tag{11}$$

$$\frac{\partial \dot{a}}{\partial f_\theta} = c_1\,(1 + e\cos\nu)\,, \tag{12}$$

$$\frac{\partial \dot{e}}{\partial f_r} = c_2 \sin\nu\,, \tag{13}$$

$$\frac{\partial \dot{e}}{\partial f_\theta} = c_2\,(\cos\nu + \cos E) \tag{14}$$

where

$$c_1 = \frac{2ah}{\mu\,(1-e^2)}\;;\; c_2 = \frac{h}{\mu}. \tag{15}$$

In the expressions above, ν is the true anomaly, E is the eccentric anomaly and h denotes the specific orbital angular momentum. Taking the derivative of Eq. (6) with respect to β provides

$$\frac{\partial \mathbf{f}}{\partial \beta} = f_{\max} \left[\begin{array}{c} \cos\beta \\ -\sin\beta \end{array} \right]. \tag{16}$$

Combining Eqs. (7), (8), (10) and (16) gives the relationship for the optimal thrust angle:

$$\nabla \Im^T \cdot \mathbf{R} \cdot \frac{\partial \mathbf{f}}{\partial \beta} = 0. \tag{17}$$

Let $\nabla \Im^T \cdot \mathbf{R} = \left[\begin{array}{cc} b_1 & b_2 \end{array} \right] = \mathbf{b}^T$. Vector $\mathbf{b}$ is a function of the current state of the system and does not depend on the thrust setting. Its components can be determined at each point of the trajectory. Once $\mathbf{b}$ is known, Eq. (17) can be solved for the thrust angle

$$b_1 \cos\beta - b_2 \sin\beta = 0 \;\;\rightarrow\;\; \beta = \arctan\frac{b_1}{b_2}. \tag{18}$$

Equation (18) gives two distinct values of β spread 180° apart. The correct one is determined from the condition

$$\mathbf{b}^T \cdot \mathbf{f} < 0\;; \tag{19}$$

the other value obviously corresponds to the maximum rate of increase of the error.

FROM JUPITER TO SATURN

The typical time scale of a two-body transfer from Jupiter to Saturn is thousands of days (years). On the other hand, the orbital periods of the two planets are 11.9 and 29.5 years, respectively. Therefore, departure time shall be chosen suitably to make sure that the spacecraft encounters Saturn at arrival. In this preliminary analysis, however, we have assumed that the error function depends only on the semimajor axis and eccentricity of the heliocentric orbit of the spacecraft, i.e., $\Im(a, e)$, and we have solved for the transfer from Jupiter to the orbit of Saturn. In other words, we have not dealt with the choice of departure time.

Upon exiting the sphere of influence of Jupiter, an electrical thruster imparts an acceleration of constant magnitude $2.5 \cdot 10^{-5}$ m/s^2, which is equivalent to a force of 25 mN acting on a mass of 1000 kg. In the case of NEXT, this level of thrust corresponds to a specific impulse of 1400 s, a

propellant flow rate of $1.85 \cdot 10^{-6}$ kg/s and a required input power of 600 W. The appealing feature of this technology is its long lifetime, estimated in 22 000 hours or 2.5 years of operation at the highest throttling point in 2007, and later brought to 48 000 hours (5.5 years).*[15]

In the proposed mission scenario, after departing Jupiter, a constant acceleration is applied to the S/C for 2.5 years (this is a conservative approach with respect to the thruster's lifetime) in a direction varying according to the above control algorithm applied to the requirement (error function) of minimizing the excess velocity of the S/C with respect to Saturn's orbit. When the thruster is deactivated, the S/C coasts until arrival. The error function is the square of the excess velocity

$$\Im(a, e) = V_{ex}^2 = \|\mathbf{V} - \mathbf{V}_S\|_{r=r_S}^2 , \tag{20}$$

where the subindex S denotes values of Saturn's orbit:

$$r_S = 9.537AU \ ; \ \mathbf{V}_S = \sqrt{\frac{\mu}{r_S}}\mathbf{u}_\theta. \tag{21}$$

To improve the accuracy of the calculations, it is advisable to use dimensionless variables. In our case, we use as reference length the astronomical unit and as reference time one year. The dimensionless value of the gravitational parameter of the Sun is thus $4\pi^2$. The square of the velocity of the probe upon intersecting Saturn's orbit is

$$V^2 = \mu\left(\frac{2}{r_S} - \frac{1}{a}\right). \tag{22}$$

Note that Eq. (22) is only physically meaningful if the trajectories of the probe and planet actually intersect, which is not a given. However, for the time being, we shall assume that this is the case. The situation where there is no intersection will be addressed later with a minor change of the expressions. From the conservation of angular momentum, the circumferential velocity of the probe at intersection is

$$V_\theta^2 = \frac{\mu a\left(1 - e^2\right)}{r_S^2}. \tag{23}$$

The radial velocity of the probe is obtained combining Eqs. (22) and (23):

$$V_r^2 = V^2 - V_\theta^2. \tag{24}$$

The error function becomes

$$\Im(a, e) = \left(V_\theta - V_S\right)^2 + V_r^2, \tag{25}$$

and its variation is

$$\delta V_{ex}^2 = 2\left(V_\theta - V_S\right)\delta V_\theta + 2V_r\delta V_r. \tag{26}$$

From Eq. (24) we obtain the variation of radial velocity at intercept

$$V_r\delta V_r = V\delta V - V_\theta\delta V_\theta, \tag{27}$$

where the change in velocity magnitude comes from Eq. (22)

$$2V\delta V = \frac{\mu}{a^2}\delta a. \tag{28}$$

*https://www.nasa.gov/centers/glenn/news/pressrel/2013/13-021_thruster.html#.XCXYplX7TIU

Using Eq. (23), we can compute the variation of circumferential velocity:

$$2V_\theta \delta V_\theta = \frac{\mu}{r_S^2}\left[(1-e^2)\delta a - 2ae\delta e\right]. \tag{29}$$

Combining Eqs. (27)-(29) gives

$$2V_r \delta V_r = \mu\left[\left(\frac{1}{a^2} - \frac{1-e^2}{r_S^2}\right)\delta a + \frac{2ae}{r_S^2}\delta e\right]. \tag{30}$$

Finally, we obtain the gradient of the error function from Eqs. (26), (29) and (30):

$$\delta\Im = \delta V_{ex}^2 = \mu\left[\begin{array}{cc}\left(\frac{1}{a^2} - \frac{1-e^2}{r_S^2}\frac{V_S}{V_\theta}\right) & \frac{2ae}{r_S^2}\frac{V_S}{V_\theta}\end{array}\right]\cdot\left[\begin{array}{c}\delta a\\ \delta e\end{array}\right] = \nabla\Im^T\cdot\delta\mathbf{o}. \tag{31}$$

In case the trajectories of the planet and S/C do not intersect, Eq. (24) gives an imaginary value for the radial velocity. This is easily fixed using

$$V_r^2 = \left|V^2 - V_\theta^2\right|. \tag{32}$$

Note that Eq. (32) gives components of the velocity which are not physical, but a useful value of the error function is obtained nonetheless (it is no longer the hyperbolic excess velocity, but it decreases as the probe's trajectory tends to the planet's orbit). With this change, the error function gradient for orbits that do not intersect becomes

$$\nabla\Im|_{NI} = \mu\left[\begin{array}{c}\frac{1-e^2}{r_S^2}\left(2 - \frac{V_S}{V_\theta}\right) - \frac{1}{a^2}\\ \frac{2ae}{r_S^2}\left(\frac{V_S}{V_\theta} - 2\right)\end{array}\right]. \tag{33}$$

Note that V_θ in Eqs. (31) and (33) is always computed using Eq. (23) regardless of whether the value is realistic or not. Direct use of Eqs. (31) and (33) leads to poor performance of the guidance algorithm, as the gradients are not continuous when the orbits of the probe and the planet are tangent (i.e., when the aphelion r_α of the probe equals the orbital radius of the planet). The error surface, when visualized in 3D, presents a very narrow valley (a sharp edge, actually). This forces the steepest descent algorithm into a zigzag path along the line of discontinuity, degrading the performance. This is a common problem with steepest descent methods, usually mitigated with an inertia term for the direction of motion (the thrust angle, in our case). For our application, however, there is a much more elegant solution. The correct path to follow when the gradient discontinuity problem arises can be determined beforehand. It is precisely the curve

$$r_\alpha = a(1+e) = r_S. \tag{34}$$

To this end, once the probe's trajectory intersects Saturn's orbit, the guidance algorithm switches to aphelion hold mode. The thrust direction is chosen in such a way that, at the end of the current time step, the predicted aphelion coincides with the orbit of the planet. That is:

$$r_\alpha + \frac{\mathrm{d}r_\alpha}{\mathrm{d}t}\Delta t = r_S, \tag{35}$$

where Δt is the time step of the numerical integrator. We can rearrange Eq. (35) as

$$\frac{\mathrm{d}r_\alpha}{\mathrm{d}t} = \frac{r_S - r_\alpha}{\Delta t} = \bar{\dot{r}}_\alpha, \tag{36}$$

which expands into

$$\nabla r_\alpha \cdot \frac{\mathrm{d}\mathbf{o}}{\mathrm{d}t} = \bar{\dot{r}}_\alpha \text{ where } \nabla r_\alpha = \begin{bmatrix} 1+e \\ a \end{bmatrix}. \tag{37}$$

Using Eq. (10)

$$\nabla {r_\alpha}^T \cdot \mathbf{R} \cdot \mathbf{f} = \bar{\dot{r}}_\alpha. \tag{38}$$

Let $\nabla {r_\alpha}^T \cdot \mathbf{R} = \begin{bmatrix} d_1 & d_2 \end{bmatrix}$. Upon substituting Eq. (6), Eq. (38) becomes

$$d_1 \sin\beta + d_2 \cos\beta = \frac{\bar{\dot{r}}_\alpha}{f_{\max}} = d_3. \tag{39}$$

To solve this equation, let us define

$$l = \sqrt{d_1^2 + d_1^2} \;\; ; \;\; \gamma = \arctan\frac{d_1}{d_2}, \tag{40}$$

such that

$$d_1 = l\sin\gamma \;\; ; \;\; d_2 = l\cos\gamma. \tag{41}$$

Substituting in Eq. (39)

$$l\left(\sin\gamma\sin\beta + \cos\gamma\cos\beta\right) = d_3. \tag{42}$$

Thus

$$\cos\left(\gamma - \beta\right) = \frac{d_3}{l} \;\; \rightarrow \;\; \beta = \gamma \pm \arccos\left(\frac{d_3}{l}\right). \tag{43}$$

From the two solutions* of Eq. (43), choose the value of β that causes the fastest rate of decrease of the excess velocity. Let β_1 be the correct choice, then

$$\left.\frac{\mathrm{d}V_{ex}^2}{\mathrm{d}t}\right|_{\beta_1} < \left.\frac{\mathrm{d}V_{ex}^2}{\mathrm{d}t}\right|_{\beta_2}. \tag{44}$$

In aphelion hold mode V_{ex} can be computed with a simpler expression:

$$V_{ex}^2 = \frac{\mu}{r_S}\left(\sqrt{2 - \frac{r_S}{a}} - 1\right)^2, \tag{45}$$

because $r_\alpha \simeq r_S$ at all times.

After applying the control law to all the cases of Figure 1, we have analysed the performance of the best solution of each set. Figure 2 gives the history of semimajor axis, eccentricity, aphelion distance and arrival excess velocity over the 2.5 years of thruster operation. Note that for the NI set the excess speed takes physical meaning only when the aphelion of the osculating orbit reaches the orbit of Saturn. Figure 3 shows the thrust angle (β) evolution for the best solution of each set. Finally, Figure 4 illustrates the two best transfers: the Earth-to-Jupiter portion, the post-GA ellipse that the S/C would follow if propulsion were not activated, the low-thrust transfer and the final Keplerian orbit till aphelion.

*Clearly, Eq. (43) is not valid if $|d_3| > l$. This means the aphelion error is too large to be corrected in a single time step. In that case, use $\beta = \gamma$ and proceed normally.

DISCUSSION

The two optimal solutions presented above correspond to similar states at the Earth (semimajor axis and eccentricity of 3.1024 ua and 0.6777 for the IN case and 3.1014 ua and 0.6776 for NI) and Jupiter (r_π = $1.6 \cdot 10^6$ km). The aphelia of the post-GA Keplerian orbits are slightly above (for the IN case) and below (for the NI case) Saturn's orbit. However, the two post-LT Keplerian orbits have approximately the same semimajor axis (7.295 ua) and eccentricity (0.3073). When the aphelion of the trajectory does not coincide with Saturn's orbital radius, the fastest way of reducing the error function is to change the semimajor axis in order to make the two orbits tangent. This process is extremely fast and consumes only a small part of the complete thrust arc. Most of the propulsion budget is spent circularizing the orbit once the aphelion coincides with the radius of Saturn's orbit. Therefore, after a swift initial correction of the semimajor axis, the two trajectories evolve very closely during the circularization stage and yield very similar final states.

The time of flight from the Earth to Jupiter is of 2.72 and 2.69 years, respectively, in the IN and NI case. In both solutions, the Jupiter-to-Saturn transfer takes 7.96 years, split into 2.5 years of LT transfer and 5.46 years of coasting time.

Note that some of the trajectories of Figure 1 have lower initial hyperbolic excess velocity than the optimal solution of the IN set. In all these cases, the eccentricity of the post-GA ellipse is higher than that of the best solution. Our experiments show that changing the eccentricity requires a larger impulse than modifying the semimajor axis. Note, however, that the error function is very smooth in the area around the optimal initial conditions. Therefore, some of the solutions that initially show greater promise yield a final excess velocity that is within one part in a thousand of the absolute minimum. In practical terms, they are equally satisfactory. With an arrival excess speed of 1.618 km/s, capture can be achieved with an OI maneuver of 175 m/s if the pericenter altitude and post-OI orbital period are those of Cassini (20 000 km and 120 days, respectively). With a constant acceleration of $2.5 \cdot 10^{-5}$ m/s^2, the ΔV accumulated during the LT portion of the transfer is of 1.972 km/s, corresponding to 146 kg of propellant at a flow rate of $1.85 \cdot 10^{-6}$ kg/s.

Under these conditions, the NEXT thruster operates at 600 W of input electrical power. At these heliocentric distances, the propulsion system cannot run on photovoltaics, given the very feeble radiation flux (14.8 W/m^2). Currently, the only viable and reliable alternative is using radioisotope thermoelectric generators (RGTs). The standard RTG in all NASA's deep space missions employs Pu^{238}, producing 285 W at beginning of life and 255 after 5-10 years of operation with a mass of 55 kg. A suite of three RTGs would satisfy the above electrical power demand with little impact on the mass budget and leave some margin for other activities. After arrival at Saturn, the electrical power system could be entirely employed to power the S/C in the scientific part of the mission.

The optimization algorithm offers a reasonable performance on commodity CPU's. Analyzing a set of 34 000 initial conditions takes 4.3 CPU seconds in a current laptop processor (Core i7-8750H).

CONCLUSIONS

This contribution presents a method to decrease the hyperbolic excess speed of a S/C approaching Saturn and facilitate the gravitational capture. The interplanetary trajectory includes a gravity assist at Jupiter, followed by a low-thrust maneuver of 2.5 years duration, compatible with the lifetime and performance characteristics of the NEXT thruster. The control law is, in essence, an application of the classical gradient descent optimization technique. In our implementation, the algorithm modifies the direction of thrust to make the semimajor axis and the eccentricity of the post-GA orbit evolve

in such a way as to minimize the arrival excess speed. Our results show that with launch energies (C_3) in the 77-85 km^2/s^2 range and with less than 150 kg of propellant, it is possible to achieve an arrival excess speed of 1.6 km/s, resulting in a OI ΔV of 175 m/s to be supplied at a pericenter altitude of about 20 000 km in order for the capture orbit to have a period of 120 days. The power needed by the electrical thruster (600 W) can be provided by a system composed of three RTGs, and this proves the technological feasibility of the concept. Future work includes the extension of the study to different magnitudes and durations of thrust and different performance parameters of the propulsion system. The methods and technologies to execute the OI maneuver will also be addressed.

ACKNOWLEDGMENT

The work of E. Fantino and J. Peláez has been supported by Khalifa University of Science and Technology's internal grants FSU-2018-07 and CIRA-2018-85. Authors of the Space Dynamics Group thank also the support provided by the project entitled Dynamical Analysis of Complex Interplanetary Missions with reference ESP2017-87271-P, supported by Spanish Agencia Estatal de Investigación (AEI) of Ministerio de Economía, Industria y Competitividad (MINECO), and by European Found of Regional Development (FEDER).

REFERENCES

[1] C. B. Phillips and R. T. Pappalardo, "Europa Clipper mission concept: Exploring Jupiter's ocean moon," *Eos, Transactions American Geophysical Union*, Vol. 95, No. 20, 2014, pp. 165–167.

[2] O. Grasset, M. Dougherty, A. Coustenis, E. Bunce, C. Erd, D. Titov, M. Blanc, A. Coates, P. Drossart, L. Fletcher, *et al.*, "JUpiter ICy moons Explorer (JUICE): An ESA mission to orbit Ganymede and to characterise the Jupiter system," *Planetary and Space Science*, Vol. 78, 2013, pp. 1–21.

[3] T. Goodson, D. Gray, Y. Hahn, and F. Peralta, "Cassini maneuver experience-Launch and early cruise," *Guidance, Navigation, and Control Conference and Exhibit*, 1998.

[4] M. W. Lo, S. D. Ross, M. Lo, and S. Ross, "The Lunar L1 Gateway: Portal to the Stars and Beyond," Albuquerque, New Mexico, AIAA Space 2001 Conference, August 2001.

[5] Y. Ren, P. Pergola, E. Fantino, and B. Thiere, "Optimal low-thrust transfers between libration point orbits," *Celestial Mechanics and Dynamical Astronomy*, Vol. 112, Jan. 2012, pp. 1–21, 10.1007/s10569-011-9382-y.

[6] E. Fantino and F. van Leeuwen, "Modelling the Torques Affecting the Hipparcos Satellite," *Space Science Reviews*, Vol. 108, Oct. 2003, pp. 499–535, 10.1023/A:1026223901234.

[7] F. van Leeuwen and E. Fantino, "Introduction to a Further Examination of the Hipparcos Data," *Space Science Reviews*, Vol. 108, Oct. 2003, pp. 447–449, 10.1023/A:1026278631277.

[8] M. L. Cosmo and E. C. Lorenzini, "Tethers in Space Handbook," tech. rep., NASA Marchall Space Flight Center, 1997.

[9] J. R. Sanmartín, M. Charro, H. B. Garrett, G. Sánchez-Arriaga, and A. Sánchez-Torres, "Analysis of tether-mission concept for multiple flybys of moon Europa," *Journal of Propulsion and Power*, Vol. 33, 2017, pp. 338—342, 10.2514/1.B36205.

[10] J. Sanmartín, J. Peláez, and I. Carrera-Calvo, "Comparative Saturn-Versus-Jupiter Tether Operation," *Journal of Geophysical Research: Space Physics*, Vol. 123, No. 7, 2018, pp. 6026–6030.

[11] D. A. Herman, "NASA's Evolutionary Xenon Thruster (NEXT) Project Qualification Propellant Throughput Milestone: Performance, Erosion, and Thruster Service Life Prediction After 450 kg," tech. rep., Glenn Research Center, Cleveland, Ohio, 2010.

[12] M. S. Bhat and S. K. Shrivastava, "An optimal Q-guidance scheme for satellite launch vehicles," *Journal of Guidance, Control, and Dynamics*, Vol. 10, No. 1, 1987, pp. 53–60.

[13] A. Cauchy, "Méthode générale pour la résolution des systémes d équations simultanées," *C. R. Acad. Sci. Paris*, Vol. 25, 1847, pp. 536–538.

[14] R. Biesbroek, *Lunar and Interplanetary Trajectories*, ch. 2, pp. 19–39. Springer, Cham: Springer Praxis Books, 2016.

[15] J. Van Noord, "Lifetime assessment of the NEXT ion thruster," *43rd AIAA/ASME/SAE/ASEE Joint Propulsion Conference & Exhibit*, 2007. 8-11 July, Cincinnati, OH.

APPENDIX: FIGURES

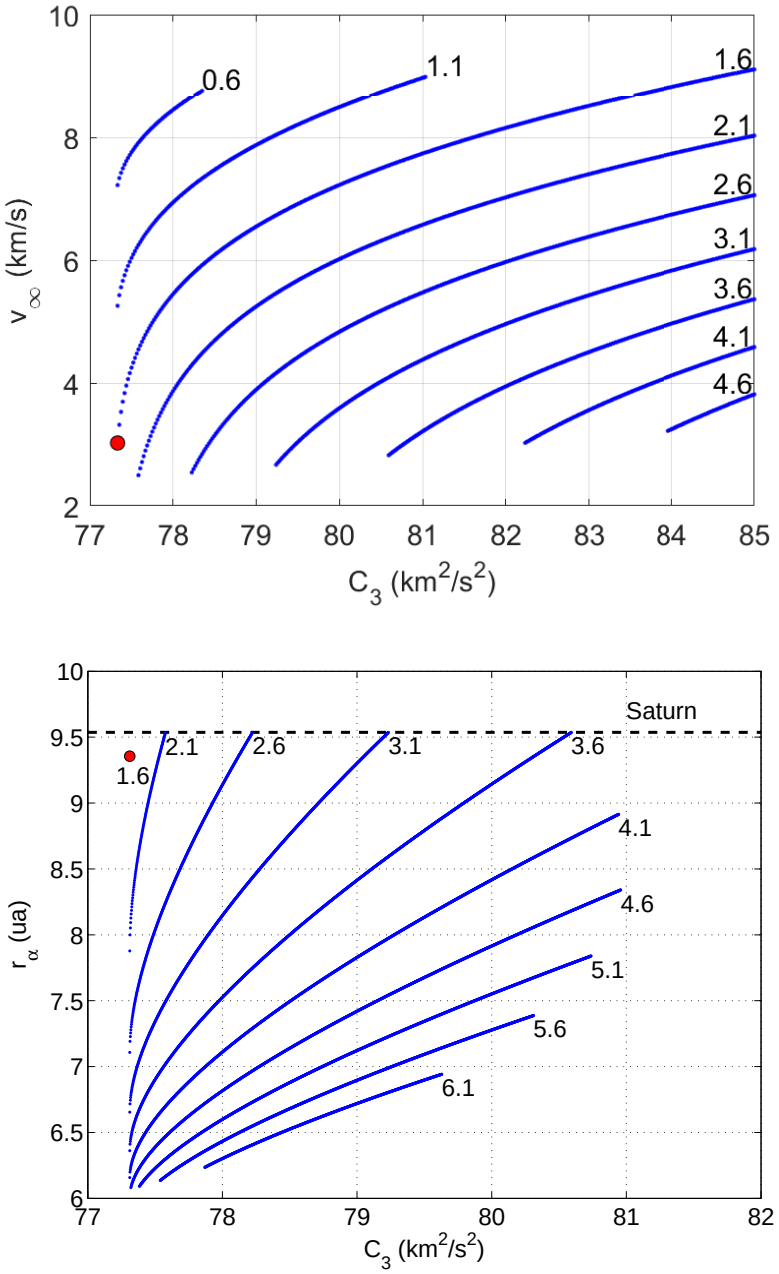

Figure 1. Hyperbolic excess speed at Saturn's orbit (top) and post-GA aphelion distance (bottom) as functions of launch C_3 for the IN and NI sets of orbits, respectively. The curves are labelled with the perijove radius in units of 10^6 km. The red solid circles indicate the trajectories which, following application of the guidance law, give the minimum arrival excess speed. The dashed line in the bottom plot indicates the radius of the orbit of Saturn.

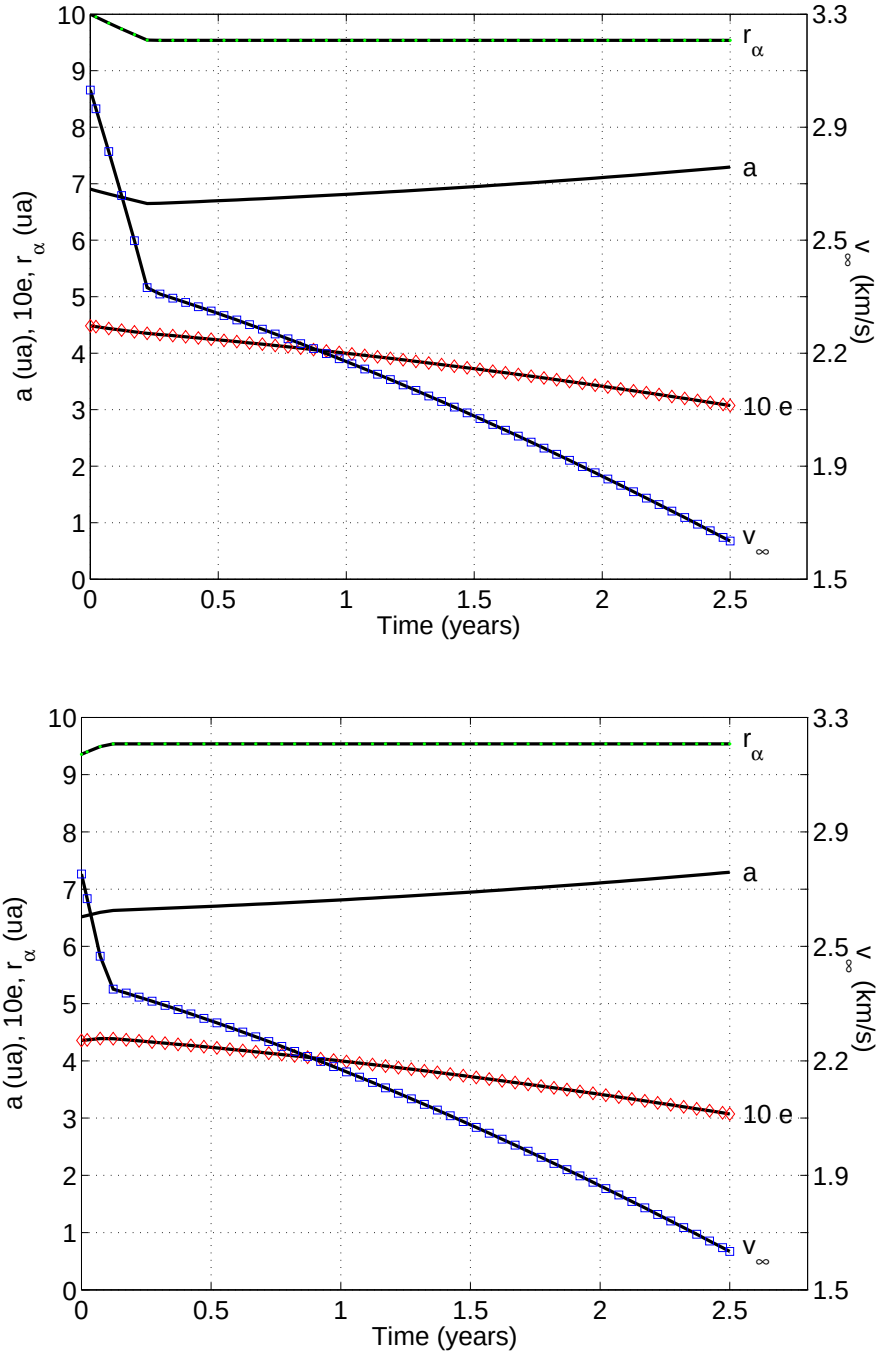

Figure 2. History of semimajor axis, eccentricity, aphelion distance and arrival excess speed over the 2.5 years of thruster operation for the best solutions of the two sets (top: IN; bottom: NI). Note that for the NI case the excess speed takes physical meaning only when the aphelion of the osculating orbit reaches the orbit of Saturn.

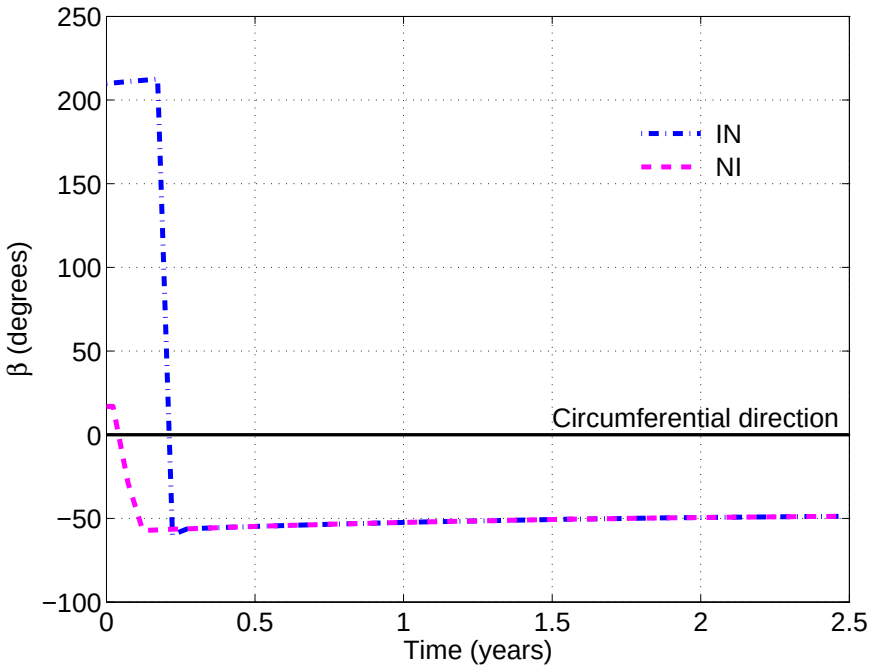

Figure 3. Thrust angle history for the two best solutions. $\beta = 0^\circ$ **corresponds to thrusting in the circumferential direction.**

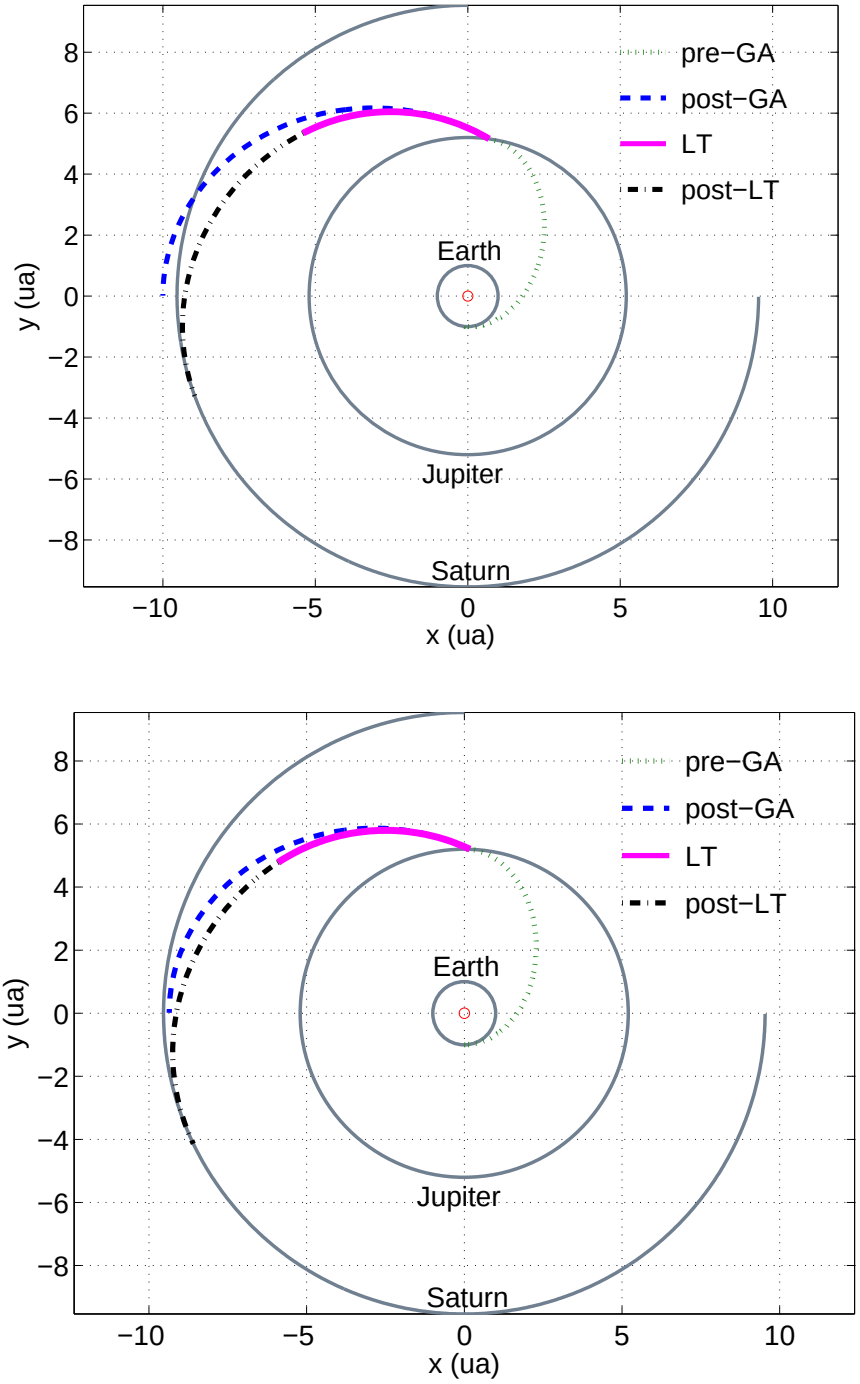

Figure 4. Trajectory followed by the S/C on the best transfer of each set (top: IN; bottom: NI): the Earth-to-Jupiter portion (pre-GA), the post-GA ellipse that the S/C would follow if propulsion were not activated, the low-thrust transfer (LT) and the final Keplerian orbit till aphelion (post-LT).